Medium-resolution *s*-process Element Survey of 47 Tuc giant stars

C.C. Worley[A,D] *and P.L. Cottrell*[B,C]

[A] Observatoire de la Côte d'Azur, B.P.4229, Nice, Cedex 04, France
[B] The Beatrice Tinsley Institute, Dept. of Physics & Astronomy, University of Canterbury, Private Bag 4800, Christchurch, New Zealand
[C] Max Planck Institut für Astrophysik, Karl-Schwarzschild Str 1, 85741, Garching, Germany
[D] Email: cworley@oca.eu

Accepted for publication in PASA, October 2011

Abstract:
Medium-resolution (R∼6,500) spectra of 97 giant stars in the globular cluster 47 Tucanæ (47 Tuc) have been used to derive the C and N abundance sensitive index, δC, and to infer abundances of several key elements, Fe, Na, Si, Ca, Zr and Ba for a sample of 13 of these stars with similar $T_{\rm eff}$ and $\log g$. These stars have stellar properties similar to the well-studied 47 Tuc giant star, Lee 2525, but with a range of CN excess (δC) values which are a measure of the CN abundance. The δC index is shown to be correlated with Na abundance for this sample, confirming previous studies. The Fe, Ca, Si and the light- and heavy-*s* process (slow neutron capture) elements, Zr and Ba respectively, have a narrow range of abundance values in these stars, indicative of a homogeneous abundance within this population of stars. The constancy of many element abundances (Fe, Si, Ca, Zr, Ba) and the δC and Na abundance correlation could imply that there has been a second era of star formation in this cluster that has revealed the products of CNO cycle burning via hot bottom burning (depletion of C, enhancement of N and the production of Na for high δC population). But there is no overall metallicity change across the range of δC values at a given position in the HR diagram that has been seen in some other globular clusters.

Keywords: globular clusters: individual (47 Tuc) – stars: abundances – stars: late-type

1 Introduction

Globular clusters (GC) are relics of the birth of the Milky Way galaxy. Their ages, if the order of the age of the Universe, mean that they hold information about early stellar and galactic formation and evolution processes. In particular as closed systems, their chemical evolution can be explored through the chemical signatures of their current stellar components. These signatures are a combination of current nuclear processes within the observed stars and of the material from which these stars formed, and hence of the previous generations of stars that polluted the intra-cluster medium. These signatures are comprised of both light and heavy element abundances, and it is by disentangling these signatures that the pollution and evolution events of GCs can be revealed.

A key goal of our survey of 47 Tuc giant stars was to ascertain the feasibility of determining *s*-process element abundances from spectra obtained at the optimal resolution of AAOmega (R∼8,000). These *s*-process elements are produced via the slow (compared to β-decay rate) accumulation of neutrons onto iron seed nuclei that can produce all the elements up to lead. Previous high resolution studies of *s*-process elements in 47 Tuc were limited to samples of less than 10 stars. Worley et al. (2010) and Wylie et al. (2006) respectively observed homogeneities and variations in the *s*-process abundance distributions. A statistically significant sample is necessary in order to truly characterise the *s*-process abundance distribution of 47 Tuc. This survey was designed to test the resolution limits of abundance determination for weak *s*-process features in giant stars.

Our survey was also designed to obtain light element abundances alongside the *s*-process elements for a more complete chemical analysis of these stars. There are several key light elemental abundance anomalies that have been observed in globular cluster stars, in particular relating to variations in carbon, nitrogen, oxygen, sodium, magnesium and aluminium. Initially, from low resolution spectra, indices on the CN and CH molecular bands determined an anti-correlation between CH and CN in globular cluster stars (Norris & Freeman 1979), whereby CN-weak stars are defined generally as having solar C and N abundances, while for CN-strong star N is enhanced by up to +1 dex and C is depleted by ~ -0.4 dex (Cannon et al. 2003).

Further study on the CN bimodality showed that while some clusters showed evidence of both CN-weak and CN-strong stars at all stages of evolution (e.g. 47 Tuc, Cannon et al. 1998), others had only one or the other at different stages, although typically both were present on the red giant branch (RGB) (Gratton et al. 2004, and references therein). The bimodality was noted to be fairly consistent from the main sequence (MS) to the RGB for any particular globular cluster, but the main discrepancy came in the asymptotic

giant branch (AGB) stars where the number of CN-strong stars decreased significantly or there were none at all (Campbell et al. 2006; Sneden et al. 2000). It was noted that this could simply be due to a lack of observations of AGB stars, and that increasing the AGB sample to compare to those from the RGB may bear useful results. Campbell et al. (2010) presented preliminary results on such an observational programme which significantly increased the sample sizes of AGB stars for 10 GCs. The preliminary results confirmed that AGB stars in GCs tended to be, in the majority, CN-weak.

Variations in O, Na, Al and Mg have also been observed and appear to be related to the variations in C and N (Cottrell & Da Costa 1981). H-burning via the CNO, NeNa and MgAl cycles affects the abundances of all of these elements. The variations that have been observed are consistent with CNO cycle processing, where Na, Al and Mg are correlated to CN-strength, while O is anti-correlated. However, the observed variations also seem to be correlated with the cluster metallicity. The correlation of Na, Al and Mg with CN-strength is seen in metal-poor clusters, that of Na and Al with CN-strength in less metal-poor clusters and only Na is correlated with CN-strength in metal-rich clusters (Gratton et al. 2004).

These variations in light elements can be attributed to H-burning via CNO cycle during hot bottom burning in intermediate mass AGB stars. Sufficiently high temperatures exist at the bottom of the envelope (top of the H-burning shell) in these stars that allow these events to occur (Cottrell & Da Costa 1981). The CN bimodality in particular is thought to be evidence of a previous generation of CN-weak stars polluting the star forming material such that the CN-strong population are born with material already fully processed in the CNO cycle. The thermally pulsing stage of AGB evolution is also responsible for producing enhancements in light and heavy *s*-process elements (Karakas & Lugaro 2010).

2 Observations

In October 2008 ninety-seven giant stars in 47 Tuc were observed using AAOmega on the AAT (Sharp et al. 2006). The target stars were selected from: Lee (1977); Paltoglou & Freeman (1984); Brown & Wallerstein (1992); Wylie et al. (2006); and Worley et al. (2008). Photometry was provided by G. Da Costa and F. Grundahl (private communication). The co-ordinates of the sample were verified using 2MASS (Skrutskie et al. 2006) where J and K magnitudes were also obtained[1].

Figure 1 shows the location of the 47 Tuc survey stars in the V-$(B-V)$ colour-magnitude diagram (CMD). The mask configurations for AAOmega restricted stars to within a 2 magnitude range. In order to obtain stars on the tip of the AGB and on the RGB below the horizontal branch (HB), the range of magnitudes for this survey was $12.5 \leq V \leq 14.5$. Hence there were some stars from either Brown & Wallerstein (1992) or Wylie et al. (2006) that could not be observed as they were outside this magnitude range.

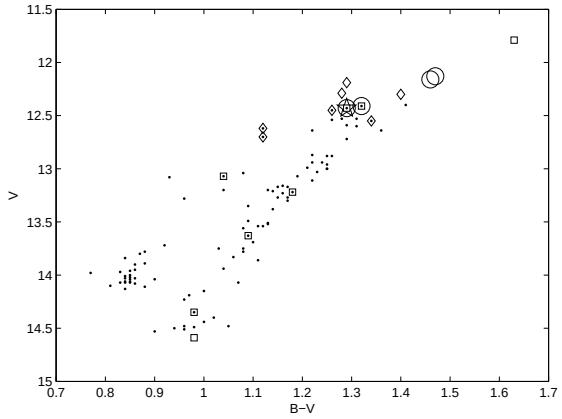

Figure 1: Colour-magnitude diagram of the 47 Tuc stars observed in the AAOmega medium resolution survey (•). Stars from Brown & Wallerstein (1992) (◯), Wylie et al. (2006) (◊) and Worley et al. (2008) (□), as well as Lee 2525 (star) are shown.

Table 1: Wavelength regions and key spectral features observed in the AAOmega 47 Tuc survey.

Camera:Grating Regions	Features (Å)
Blue:3200B	
$\lambda\lambda$ 4040 - 4350 Å	CN (4142 - 4216)
	CH (4300 - 4330 G Band)
Red:2000R	
$\lambda\lambda$ 5750 - 6200 Å	Na I (6154.23, 6160.75)
	Si I (6131.57, 6131.85, 6145.02, 6155.13)
	Ca I (6156.02, 6166.44, 6169.56)
	Fe I (6147.83, 6157.73)
	Zr I (6143.18)
	Ba II (6141.73)
	La II (5805.77)
	Nd II (5811.57)

AAOmega has a red and a blue camera with which stars can be observed simultaneously over two distinct wavelength ranges. The wavelength regions observed for this survey and the key features that have been analysed are listed in Table 1. The resolution of the spectra was $R \sim 6500$ and the signal-to-noise (SNR) per pixel ranged from 30 to 50 for the blue arm, and 60 to 90 for the red arm. The spectra were reduced using the reduction pipeline, 2dFdr[2].

[1] http://www.ipac.caltech.edu/2mass

[2] http://www.aao.gov.au/2df/manual/UsersManual.pdf

The normalisation of the spectra was treated differently for the blue and red arms. The key features in the blue arm observations were CN and CH molecular bands that obscure the location of the true continuum. In the red arm observations molecular features were not so prominent at the stellar temperatures of these stars. In both cases comparison was made to the high resolution spectrum of Arcturus (Hinkle & Wallace 2005) which was convolved to a resolution comparable to the AAOmega observations. Different methods were employed in order to locate the continuum in the blue and the red.

For the red arm, the convolved Arcturus spectrum was compared with synthesised spectra generated using the Arcturus stellar model determined in Worley et al. (2009). Using the spectrum synthesis programme MOOG (Sneden 1973), the atomic linelist, collated from the latest laboratory values, was calibrated so that the synthetic spectrum matched the high resolution spectrum for Arcturus. The linelist was modified to include hyper-fine splitting components and isotopic ratios for barium. The abundances for each of the key lines in the red (see Table 1) were measured by spectrum synthesis for both the high- and medium-resolution spectra of Arcturus. Corrections for departures from local thermodynamic equilibrium for the two sodium features were applied after the abundance determination for each star (Lind et al. 2011). The abundances for Arcturus are listed in Table 2.

Table 2: Elemental abundances and abundance ratios with respect to the Sun derived from high (HR) and medium resolution (MR) spectra of Arcturus using spectrum synthesis.

Species	λ (Å)	χ (eV)	HR	MR
[Fe I/H]	6136.62	2.45	-0.63	-0.44
[Fe I/H]	6147.83	4.08	-0.61	-0.62
[Fe I/H]	6157.73	4.08	-0.60	-0.52
		$\langle$[Fe/H]$\rangle$	-0.61	-0.53
		σ	0.02	0.09
[Na I/Fe]	6154.23	2.10	0.13	0.02
[Na I/Fe]	6160.75	2.10	0.19	0.10
		$\langle$[Na/Fe]$\rangle$	0.16	0.06
		σ	0.04	0.06
[Si I/Fe]	6131.57	5.62	0.20	0.21
[Si I/Fe]	6131.85	5.62	0.26	0.22
[Si I/Fe]	6145.02	5.62	0.24	0.18
[Si I/Fe]	6155.13	5.62	0.24	0.41
		$\langle$[Si/Fe]$\rangle$	0.24	0.26
		σ	0.03	0.10
[Ca I/Fe]	6156.02	2.52	0.24	0.27
[Ca I/Fe]	6166.44	2.52	0.36	0.23
		$\langle$[Ca/Fe]$\rangle$	0.30	0.25
		σ	0.08	0.03
[Zr I/Fe]	6143.18	0.07	0.02	-0.12
[Ba II/Fe]	6141.73	0.70	-0.20	0.04
[La II/Fe]	5805.77	0.13	-0.01	-0.05
[Nd II/Fe]	5811.57	0.86	0.00	0.00

The Ba abundance shows the greatest change between the high-resolution and the convolved Arcutrus spectra. The Ba spectral line that was measured is very strong ($W_\lambda \approx 180$ mÅ) and so it is sensitive to changes in microturbulence. The remaining elements are in reasonable agreement to ≤ 0.15 dex between the high-resolution and convolved spectra. These variations in abundance from the high-resolution spectrum to the convolved medium-resolution spectrum provide a measure of the uncertainty in determining the abundances in medium-resolution spectra.

For the blue arm spectral region the high-resolution Arcturus atlas was compared to the convolved Arcturus spectrum in the region of the CN and CH molecular bands. This allowed us to identify pseudo- continuum regions that could be used to normalise the spectra. By enforcing a ratio between the location of three wavelength regions (around 4090Å, 4220Å and 4318Å), we created a linearly interpolated profile for each spectrum that was used to undertake the normalisation. For the spectra of 22 objects, there was no 4318Å region in the spectrum because of the instrument setup and placement of these objects in the focal plane of AAOmega. For these spectra a normalisation based on the normalisation shape for stars of similar $T_{\rm eff}$ was used.

3 CN indices

CN indices for stars in 47 Tuc have been measured in several studies. A number of stars observed in this survey were previously observed by Norris & Freeman (1979) and Paltoglou & Freeman (1984) (hereafter NF79 and PF84 respectively), in which they were classified by their CN indices, designated here as δC_{1979}. This study seeks to extend these analyses. The CN index used here (δC_{2011}) was that defined by NF79 and PF84:

$$S(4142) = -2.5 log_{10}\Big\{\frac{\int_{4120}^{4216} F_\lambda d\lambda}{\int_{4216}^{4290} F_\lambda d\lambda}\Big\}. \quad (1)$$

NF79 calibrated this line intensity version of the CN index to the previous photometric index, C(4142), using the following equation:

$$C(4142) = 0.742 \times S(4142) + 0.236. \quad (2)$$

In order to determine the CN excess, δC(4142) (hereafter δC), the CN indices were considered in C(4142)–V space in NF79, and in C(4142)–(B–V) space in PF84. Based on these studies, in this analysis we used the following equation to derive δC_{2011} for the 47 Tuc sample:

$$\delta C_{2011} = C(4142) - (0.304 \times (B-V) - 0.275). \quad (3)$$

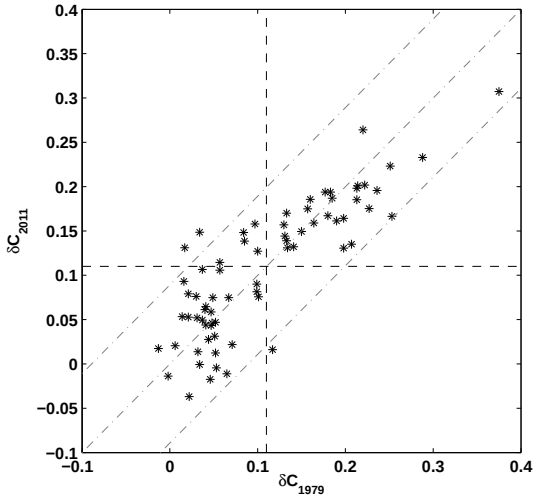

Figure 2: Comparison of CN excesses (δC), from NF79 and PF84 (on abcissa) with the values derived in this study (on ordinate). The dashed lines indicate the CN-weak, CN-strong threshold at δC = 0.11. The dash-dot lines indicate the 1:1 relation $\pm$ 2 σ.

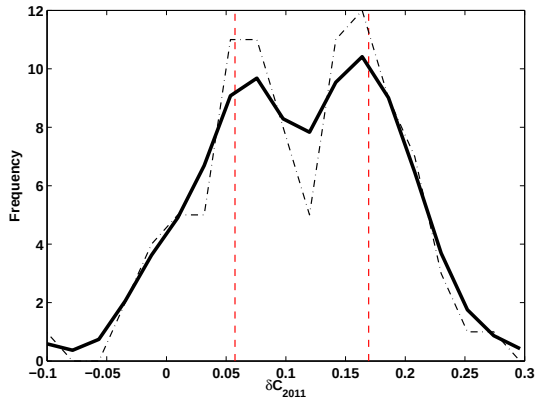

Figure 3: Frequency distribution, raw and smoothed, showing the CN bimodality in the 47 Tuc survey using the δC_{2011} values. The means of each population are shown as red lines.

The stars were classified as CN weak if $\delta C_{2011} \leq 0.11$ or CN strong if $\delta C_{2011} > 0.11$ (PF84), as shown in Figure 2. The photometry, T_{eff} and log g calculated from $V - K$, and δC_{2011} values for each star in the survey are given in Appendix A. The majority of the stars fall along the 1:1 relation with a 2 σ uncertainty. There are three stars which lie outside the 2 σ limits.

In each case the star has changed designation between CN-strong and CN-weak. Lee 1506 (δC_{2011} = 0.016) changed from CN-strong to CN-weak, whereas Lee 5703 (δC_{2011} = 0.131) and Lee 3415 (δC_{2011} = 0.149) went from CN-weak to CN-strong. The spectra of these outliers were checked for any artifact or normalisation discrepancy but in all three cases the δC_{2011} value could not be reconciled with the previous measurements. This may indicate misidentification in the previous studies as the coordinates that are used here are consistent with the coordinates of these objects as given in SIMBAD[3].

Figure 3 reduces the CN excess measurements of this study into a histogram using a bin interval of 0.02 (dotted line) and then smoothed using a gaussian filter with a full width at half maximum (FWHM) of 0.05 (solid line) that better reflects the precision of the data (c.f. NF79; PF84). The CN bimodality is seen as two peaks, one for the CN-weak stars at $\delta C_{2011} \sim 0.054$ and the other for the CN-strong stars at $\delta C_{2011} \sim 0.166$. These values are the mean (μ) values for each population that were determined by the application of a simple gaussian mixture model. The model determined $\sigma = 0.055$ for both populations in mixing proportions of 0.48 for the CN-weak population, and 0.52 for the CN-strong population. The difference in the means, $\Delta\mu = 0.112$, is slightly greater than $2\sigma = 0.11$ which is the minimum limit necessary to detect two populations in a single dataset(Reschenhofer 2001). Hence two populations in δC_{2011} exist within this dataset.

The CN-CH anti-correlation is a well known feature of 47 Tuc and other globular clusters (Cannon et al. 1998). Figure 4 compares a CN-weak and a CN-strong star of similar $T_{\rm eff}$ and *log g*. The CN bandhead (degrading to the blue from ∼4216 Å) is distinctly different between the CN-weak and CN-strong stars. At the CH band the CN-strong star has a weak CH band, corresponding to a carbon depletion and nitrogen enrichment from the CN band.

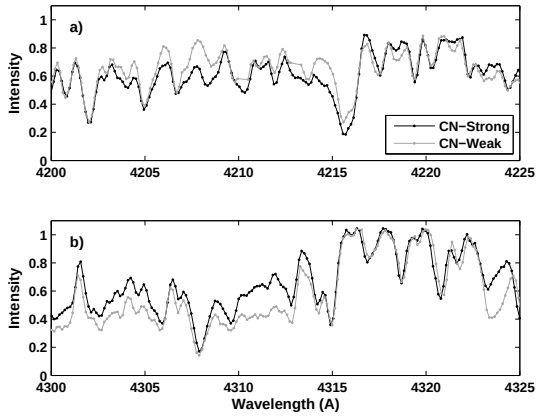

Figure 4: Comparison of a CN-weak star (grey, Lee 4506, δC_{2011}=0.050) with a CN-strong star (black, Pal 578, δC_{2011}=0.164) of similar $T_{\rm eff}$ and log g from the 47 Tuc stellar survey. (a) CN bandhead at 4216 Å. (b) G Band.

4 Atmospheric parameters

The stellar atmospheric models for each star were based on the effective temperature ($T_{\rm eff}$) and surface gravity

[3]http://simbad.u-strasbg.fr/simbad/

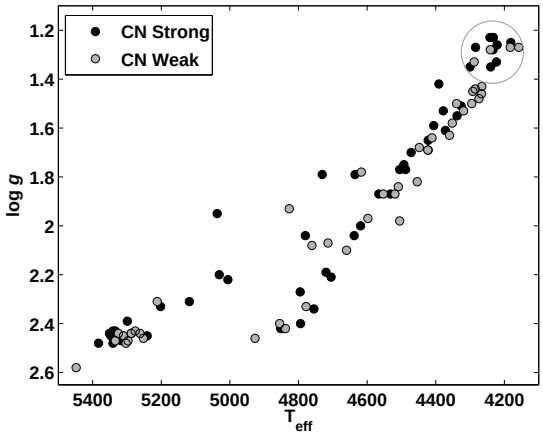

Figure 5: $T_{\rm eff} - \log g$ space for CN-weak (grey circle) and CN-strong (black circle) pairs based on V–K photometry. The circle encompasses Lee 2525-like stars.

($\log g$) values derived from the V–K photometry and using the relationships in Alonso et al. (1999). Comparison between CN-weak and CN-strong stars is ideally investigated using stars at similar $T_{\rm eff}$ and $\log g$. These are shown in $T_{\rm eff} - \log g$ space in Figure 5 and contain many pairs on the RGB, HB and AGB.

The group of thirteen stars (see circle in Figure 5) at $T_{\rm eff} \approx 4200$ K and $log\ g \approx 1.3$ includes the star Lee 2525, for which a high-resolution analysis was carried out by Worley et al. (2009). The stars in this group have approximately the same stellar parameters and provide a sample of comparable stars at different CN strengths. The stellar designations, CN excess, photometry and stellar parameters for these stars are listed in Table 3, and are analysed in the remainder of this paper.

4.1 Lee 2525

Lee 2525 is a 47 Tuc giant star that has been observed in several studies. It has been singled out as a linking star in two previous studies (Wylie et al. 2006; Brown & Wallerstein 1992). It has been observed in three separate datasets: SALT PV RSS medium resolution observations of eleven stars in 47 Tuc (Worley et al. 2008); AAOmega 47 Tuc medium resolution survey (this study); and high resolution observation of Lee 2525 on the SSO 2.3 m telescope (Worley et al. 2009). Figure 6 compares the spectra of Lee 2525 from all three studies in the regions of the light and heavy element spectral features. For comparison, the SSO high resolution spectrum was convolved to a resolution comparable to the AAOmega data in this study.

The Lee 2525 spectrum observed on RSS is at a lower resolution than the AAOmega spectra. The features in common between the high and medium resolution spectra agree in terms of their relative line depths. Abundances derived by spectrum synthesis were obtained for the light and heavy elements for each spectrum, including the convolved SSO spectrum, and are discussed in the next section.

In NF79, Lee 2525 was found to be a CN-weak star with a $\delta C_{1979} = 0.10$. Its CN-strong pair was

Table 3: Thirteen stars of similar stellar parameters are listed with their ID, CN excesses taken from NF79 and PF84 (δC_{1979}), and CN excesses calculated in this study (δC_{2011}). The stellar parameters, $T_{\rm eff}$ and $\log g$, were calculated for each star based on V–K photometry.

Star ID	δC_{2011}	δC_{1979}	Ref.	$T_{\rm eff}$	$\log g$
Pal502	-0.04	0.02	PF84	4158	1.27
Lee2306	0.00	0.05	NF79	4288	1.33
Lee3622	0.01	0.03	NF79	4183	1.27
Lee4628	0.04	0.05	NF79	4241	1.28
Lee2525	0.08	0.10	NF79	4232	1.23
W66	0.08	-	-	4181	1.25
Lee5703	0.13	0.02	NF79	4221	1.26
Lee1513	0.14	0.21	NF79	4242	1.23
W139	0.15	-	-	4223	1.33
Pal262	0.17	0.25	PF84	4240	1.35
W164	0.17	-	-	4300	1.35
Pal661	0.20	0.22	PF84	4233	1.28
Lee1747	0.22	0.25	NF79	4284	1.27
			Mean	4233	1.28
			σ	$\pm$44	$\pm$0.09

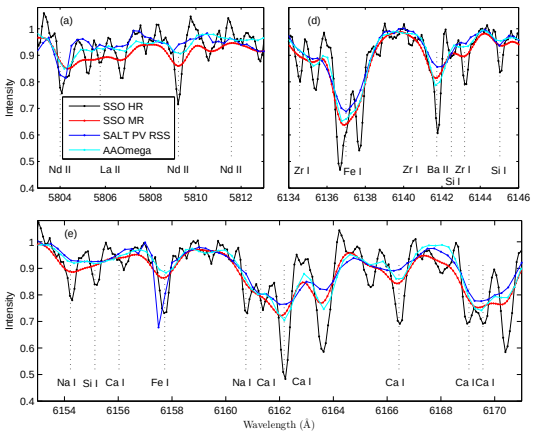

Figure 6: Comparison of the Lee 2525 spectra observed using RSS on SALT (blue), the SSO 2.3 m telescope (black), and AAOmega on the AAT (cyan). Also included is the convolution of the high resolution spectra to a resolution comparable to the AAOmega observation (red). (a) Nd II and La II features in the 5800 Å region. (b) Si I, Fe I, Ba II and Zr I features in the 6140 Å region. (c) Na I, Si I, Ca I and Fe I features in the 6160 Å region.

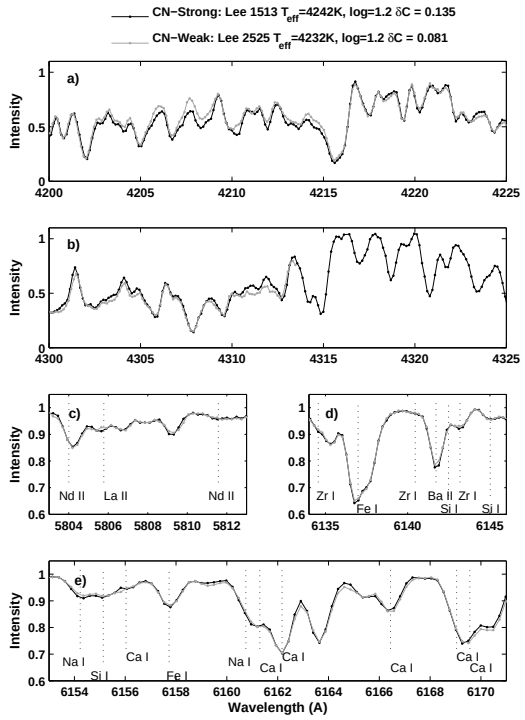

Figure 7: Comparison of Lee 2525 (grey) and Lee 1513 (black) spectra. (a) CN band, (b) CH band, (c) Nd II and La II, (d) Si I, Fe I, Ba II and Zr I, (e) Na I, Si I, Ca I and Fe I.

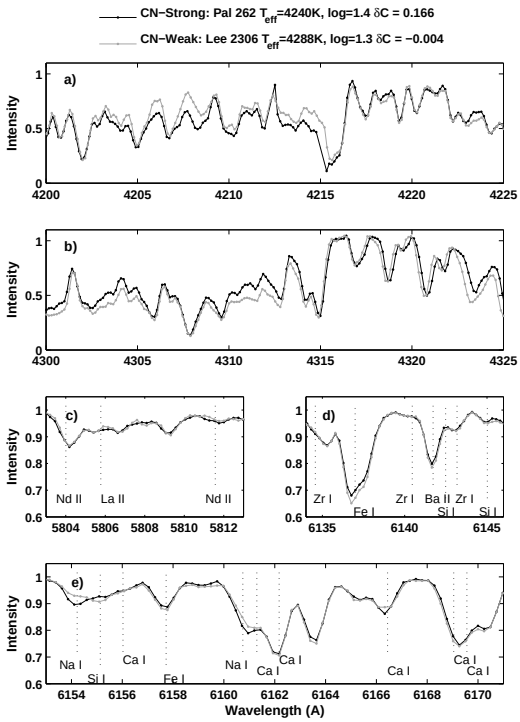

Figure 8: As for Figure 7, but comparing the spectra of Pal 262 (black) and Lee 2603 (grey).

Lee 1513 which had a CN excess of $\delta C_{1979} = 0.21$ (Brown & Wallerstein 1992). This pairing holds in the current analysis where Lee 2525 was designated as CN-weak ($\delta C_{2011} = 0.08$) and Lee 1513 as CN-strong ($\delta C_{2011} = 0.14$), although not as strong as in the previous study.

Figure 7 compares the spectra from these two stars, Lee 2525 and Lee 1513. The two spectra are strikingly similar in all regions except that the CN where the smaller δC in Lee 2525 can be discerned. The remaining spectral regions are also almost an exact match, except that the Na feature at 6154 Å is slightly enhanced in the CN-strong spectrum relative to the CN-weak spectrum.

Figure 8 compares two stars that are well separated in CN excess value but have similar overall stellar parameters. Pal 262 is a CN-strong star with $\delta C_{2011} = 0.17$, while Lee 2603 is a CN-weak star with $\delta C_{2011} = 0.00$. The differences in CN and CH strength are particularly distinct. What also becomes apparent is the difference in the line strength of the two Na I lines at 6154 Å and 6160 Å. The CN-strong star was considerably stronger in Na I lines than the CN-weak star. The correlation of Na I with CN strength has been noted in previous studies (Gratton et al. 2004; Cottrell & Da Costa 1981) and will be analysed in Section 5.1. The remaining features, in particular the *s*-process element features, show no distinct difference in line strength between these stars.

5 Lee 2525 sample analysis

The subset of stars at $T_{\rm eff} \approx 4200$ K and $\log g \approx 1.3$ was used to investigate the abundances of the light and heavy elements in 47 Tuc stars. In the high-resolution analysis of Lee 2525 (Worley et al. 2009) the stellar atmospheric model for Lee 2525 was determined to have $T_{\rm eff} = 4225$ K, $\log g = 1.2$, $\xi = 1.8$ kms^{-1} and [Fe/H] $= -0.70$ dex. This model was used in the following abundance analysis of the medium-resolution observation of Lee 2525. It was subsequently used as the model for all the remaining stars in the subset defined in Table 3 as it is within 1 σ (10 K and 0.1 dex) of the mean $T_{\rm eff}$ and $\log g$ for all of these stars.

In order to make a direct comparison, the high-resolution SSO Lee 2525 spectrum was convolved to the same resolution as the AAOmega spectrum and an abundance analysis was carried out. The results from that analysis and a spectrum synthesis analysis of the high-resolution Lee 2525 spectrum are also listed in Table 4[4].

[4]From this section onwards the definition of the bracket notation [X/H] or [X/Fe] is $\log_{10}(\rm X/H)_\star - \log_{10}(\rm X/H)_{Arcturus}$ or $\log_{10}(\rm X/Fe)_\star - \log_{10}(\rm X/Fe)_{Arcturus}$

Table 4: Elemental abundances derived for Lee 2525 from the medium-resolution (MR) AAOmega spectrum, from the spectrum convolved from the high-resolution (C-HR) SSO 2.3 m observation of Lee 2525 and from the high-resolution (HR) analysis itself. The abundances are calculated differentially with respect to the Arcturus MR or HR abundances. Error analysis on the AAOmega medium-resolution spectrum is also included for the specified changes in stellar parameter.

	Instrument Resolution	AAOmega Medium	SSO 2.3 m Convolved	SSO 2.3 m High	Δ[Fe/H]		
	λ (Å)	[Fe/H]	[Fe/H]	[Fe/H]	ΔT_{eff} +100 K	$\Delta \log g$ 0.5	$\Delta\xi$ 0.5
Fe I	6136.62	-0.13	-0.03	0.08	0.03	0.10	-0.33
Fe I	6147.83	0.02	0.11	-0.04	-0.08	0.15	-0.13
Fe I	6157.73	-0.02	0.10	0.10	-0.03	0.11	-0.26
	$\langle$[Fe/H]$\rangle$	-0.04	0.06	0.05	-0.05	0.13	-0.20
	σ	0.08	0.08	0.08	0.13	0.16	0.21
X		[X/Fe]	[X/Fe]	[X/Fe]	Δ[X/Fe]		
Na I	6154.23	0.00	0.23	0.12	0.06	-0.02	-0.09
Na I	6160.75	-0.08	-0.10	0.15	0.08	0.00	-0.12
	$\langle$[Na/Fe]$\rangle$	-0.04	0.06	0.14	0.07	-0.01	-0.11
	σ	0.06	0.23	0.02	0.01	0.01	0.02
Si I	6131.57	0.09	0.06	0.10	-0.02	0.13	0.01
Si I	6131.85	0.08	0.05	0.09	0.00	0.18	0.03
Si I	6145.02	0.07	0.22	0.06	-0.01	0.17	-0.04
Si I	6155.13	-0.12	-0.31	-0.04	-0.03	0.14	-0.08
	$\langle$[Si/Fe]$\rangle$	0.03	0.00	0.05	-0.02	0.16	-0.02
	σ	0.01	0.22	0.06	0.03	0.03	0.07
Ca I	6156.02	-0.14	-0.21	-0.14	0.05	0.03	-0.07
Ca I	6166.44	0.01	0.07	-0.11	0.13	0.09	-0.23
	$\langle$[Ca/Fe]$\rangle$	-0.07	-0.07	-0.13	0.09	0.06	-0.15
	σ	0.11	0.20	0.02	0.06	0.04	0.11
Zr I	6143.18	0.02	0.42	0.28	0.15	0.05	-0.10
Ba II	6141.73	0.26	-0.14	0.00	0.00	0.17	-0.60
La II	5805.77	-0.03	0.45	0.21	0.08	-0.08	-0.08
Nd II	5811.57	-0.20	-0.06	0.00	0.10	0.03	0.03

Table 5: Elemental abundances derived for thirteen stars in the 47 Tuc medium-resolution survey with stellar parameters similar to Lee 2525. The abundances determined for the convolved high-resolution (C-HR) Arcturus atlas are also listed and are with respect to the Sun, whereas the 47 Tuc abundances are calculated differentially with respect to these Arcturus values. The Lee 2525 stellar atmospheric model was used to infer the abundances for each of these stars. The mean abundances and standard deviations for the entire 47 Tuc sample are also listed.

Star	Arcturus	Pal502	Lee2306	Lee3622	Lee4628	Lee2525	W66	Lee5703	Lee1513
ξ	1.5	1.8	1.8	1.5	1.8	1.8	1.8	1.8	2.0
δC_{2011}	-0.06	-0.04	0.00	0.01	0.04	0.08	0.08	0.13	0.14
[Fe/H]	-0.53	-0.20	-0.14	-0.14	-0.13	-0.14	-0.15	-0.14	-0.15
[Na/Fe]	0.06	-0.06	-0.21	-0.13	-0.18	-0.10	0.06	-0.06	-0.02
[Si/Fe]	0.26	-0.06	0.02	-0.08	0.03	0.03	-0.08	-0.02	0.01
[Ca/Fe]	0.25	0.05	-0.14	0.03	-0.03	-0.07	-0.01	-0.07	-0.12
[Zr/Fe]	-0.12	0.32	0.07	0.22	0.22	0.02	0.27	0.09	0.10
[Ba/Fe]	0.04	0.21	0.24	0.29	0.31	0.26	0.21	0.36	0.29
$[hs/ls]$	0.16	-0.11	0.17	0.07	0.09	0.24	-0.06	0.27	0.19

Star	W139	Pal262	W164	Pal661	Lee1747		Sample Statistics	
ξ	1.8	1.5	1.8	1.8	1.8	$\langle\xi\rangle$	1.8	0.13
δC_{2011}	0.15	0.17	0.17	0.20	0.22	$\langle\delta C_{2011}\rangle$	0.10	0.09
[Fe/H]	-0.13	-0.16	-0.16	-0.12	-0.11	$\langle$[Fe/H]$\rangle$	-0.14	0.02
[Na/Fe]	-0.08	0.25	0.02	0.02	0.17	$\langle$[Na/Fe]$\rangle$	-0.02	0.13
[Si/Fe]	0.04	-0.01	-0.08	0.00	0.01	$\langle$[Si/Fe]$\rangle$	-0.01	0.04
[Ca/Fe]	-0.14	-0.03	-0.11	-0.09	-0.12	$\langle$[Ca/Fe]$\rangle$	-0.06	0.06
[Zr/Fe]	0.12	0.12	0.12	0.07	0.07	$\langle$[Zr/Fe]$\rangle$	0.14	0.09
[Ba/Fe]	0.26	0.31	0.36	0.26	0.26	$\langle$[Ba/Fe]$\rangle$	0.28	0.05
$[hs/ls]$	0.14	0.19	0.24	0.19	0.19	$\langle[hs/ls]\rangle$	0.14	0.11

There is reasonable agreement in the abundance for Fe for all three sets of results with a similar level of uncertainty (∼0.08 dex). For the light elements, the convolved SSO spectrum produced the largest spread in values (∼0.2 dex) between the lines for each of Na, Si and Ca, while for the other two spectra there were smaller uncertainties in each ($\leq$ 0.11 dex). Clearly the information retained in a simple gaussian convolution does not necessarily match observations at the resolution to which the convolution was made.

For each of the light and heavy elements there are discrepencies between the abundance determinations of these different Lee 2525 spectra which is an example of how the degradation of spectra to lower resolution imply a different abundance of an element. Also the high resolution spectrum of Lee 2525 had SNR∼50 so features that are due to the noise are likely to have contaminated the shape of the spectral features in the convolution. There was much better agreement between abundances derived from the Arcturus high resolution and convolved spectra (see Table 2). A high SNR, high resolution observation of Lee 2525 would provide the basis for a more consistent comparative analysis.

The error analysis in Table 4 shows changes in the elemental abundances on the order of 0.1 dex for changes in the stellar parameters based on the intervals in the stellar model grid.

With regard to the *s*-process element abundances, the spectral features for La and Nd are heavily blended at this resolution (see Figure 6) and only the Ba line at 6141.73 Å and the Zr line at 6143.18 Å looked sufficiently distinct for analysis. Abundances were determined for La and Nd for the Lee 2525 spectra, but the features were deemed to be too blended ($R \sim 6500$) for analysis in the remaining survey stars.

Following this analysis of the medium-resolution Lee 2525 spectra the other stars in Table 3 were analysed for their elemental abundances. As noted earlier, the model determined for Lee 2525 was used in the analysis of the spectra for each of these stars. The only parameter that was varied was the microturbulence (ξ_t) as it was clear for four of the stars that the Lee 2525 microturbulence value was not a good fit. Table 5 lists the stellar parameters, CN excess and elemental abundances for each of the thirteen stars in this subset. The $[hs/ls]$ ratio is included as the difference between the Ba (heavy *s*-process) and Zr (light

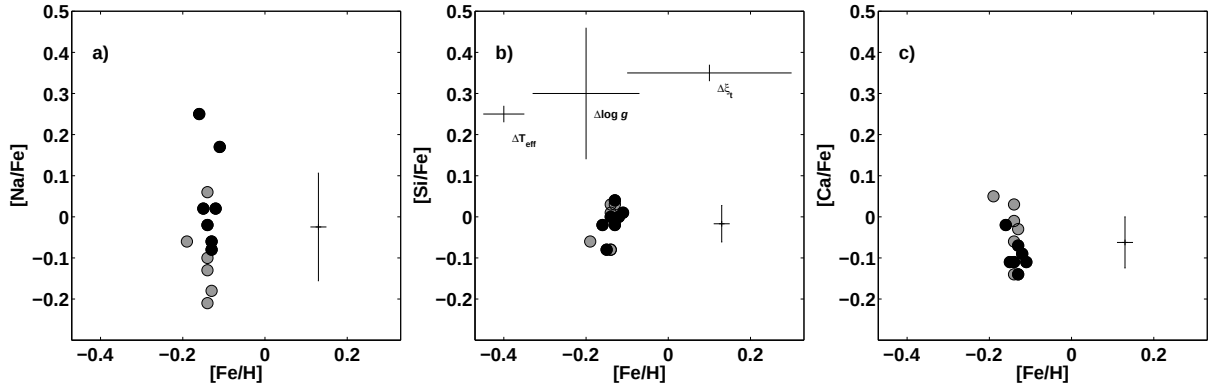

Figure 9: The element abundance ratios [X/Fe] calculated with respect to the medium resolution abundance analysis of Arcturus for a) Na, b) Si and c) Ca against [Fe/H] for each of the thirteen 'Lee 2525-like' stars. Grey circles are CN-weak stars and black circles are CN-strong. The sample mean and standard deviation for each is also shown. The systematic uncertainties from Table 4 are illustrated for [Si/Fe].

s-process) abundances.

5.1 Light elemental abundances

The light elemental abundance ratios with respect to Arcturus are compared with [Fe/H] in Figure 9. The [Si/Fe] and [Ca/Fe] abundance ratios each have a small spread (of < 0.2 dex) for this sample, indicating that there is a homogeneous abundance distribution for these two elements. The systematic uncertainties with associated changes in $T_{\rm eff}$, $\log g$ and ξ_t presented in Table 4 are shown for [Si/Fe] and [Fe/H] in Figure 9b to illustrate the range in values with changes in stellar parameters. The spread in the [Na/Fe] far exceeds what can be expected from the corresponding systematic uncertainties of ~ 0.2 dex (Table 4). This implies that the range in [Na/Fe] is real.

Furthermore the Na-CN strength correlation is well documented in globular cluster stars (Cottrell & Da Costa 1981). Figure 10 compares the [Na/Fe] abundance ratio with CN strength (δC_{2011}). There is a clear correlation, with the increasing enrichment in Na corresponding to increasing CN strength. The trend seems continuous rather than attributable to two distinct populations. Of the stars in the Lee 2525-like sample 10 have previously determined δC values, one of which is Lee 5703 for which the δC_{2011} differed above 2 σ from the δC_{1979} value. However is it not one of the outliers in the Figure 10, nor for the remaining abundance determinations, implying that the current analysis of that star is reliable.

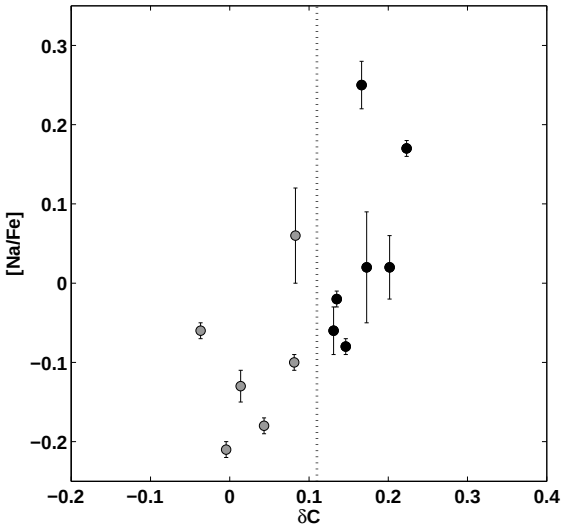

Figure 10: [Na/Fe] with respect to Arcturus against δC_{2011} for each of the thirteen Lee 2525-like stars. The dotted line shows the threshold at 0.11. Grey circles are CN-weak stars and black circles are CN-strong.

5.2 Heavy elemental abundances

Figures 11a and b show the abundance ratios for each of [Zr/Fe] and [Ba/Fe] against [Fe/H] for the Lee 2525-like sample. In Figure 11a there is a distinct spread in the values for [Zr/Fe]. However the Zr feature used in this analysis (see Figure 7) is small and quite blended at this resolution so the larger uncertainly is not unexpected. There is however a very small spread in the [Ba/Fe] abundance ratios (Figure 11b) that is similar to that for [Si/Fe] in Figure 9b. The Ba feature used here is very senstive to ξ_t. However the small spread indicates that the adjustment of the ξ_t values resulted in consistency between the Ba and Fe abundances.

Figure 11c shows the distribution of the $[hs/ls]$ ratio against [Fe/H] for this sample. The spread in [Fe/H] is very small at 0.02 dex while the larger spread in the $[hs/ls]$ values can mainly be attributed to the spread in the Zr abundances, hence they are subject to large systematic uncertainties. The sample mean value of $\langle[hs/ls]\rangle = 0.14\pm0.11$ dex is slightly higher than some recent analysis of high resolution spectra of 47 Tuc giant stars, $[hs/ls] = -0.13 \pm 0.05$ dex (Worley et al. 2010). Both of these values are indica-

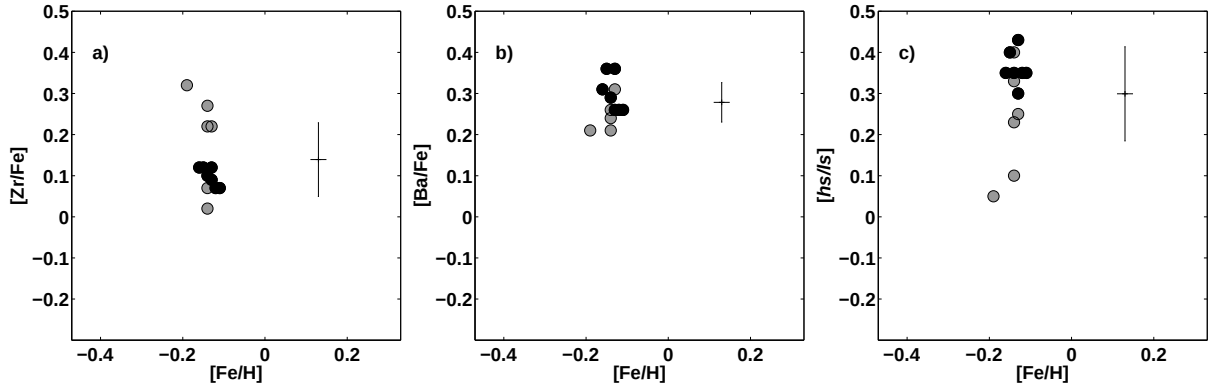

Figure 11: The abundances of the *s*-process elements with respect to Arcturus, a) Zr and b) Ba, against [Fe/H] for the thirteen Lee 2525-like stars in the 47 Tuc medium-resolution survey with sample mean and standard deviation. c) The ratio of $[hs/ls]$ against [Fe/H] for the sample. Grey circles are CN-weak stars and black circles are CN-strong.

tive of values for stars at this metallicity (Busso et al. 2001). This analysis shows that to properly survey the weak *s*-process spectral features a higher resolution is needed.

6 Conclusion

The medium-resolution survey of 47 Tuc stars has provided a good sample with which to investigate several aspects of chemical abundances in GCs. The survey sample clearly shows the CN-CH anti-correlation which is well-documented for GCs (Norris & Freeman 1979; Cannon et al. 1998, 2003; Briley et al. 2004). The bimodal distribution of CN-weak and CN-strong stars is also evident in the sample. The current measurement of the CN indices of these stars were in reasonable agreement with the previous studies of NF79 and PF84.

The grouping of stars about Lee 2525 provided a unique sample with which to investigate abundance variations for stars of very similar stellar parameters. To complement the CN indices, the medium-resolution spectra were analysed for light and heavy element abundnaces using spectrum synthesis techniques. This preliminary set of stars, and their representative star, Lee 2525, provided a link to high-resolution abundance analyses of 47 Tuc giant stars in previous studies (Wylie et al. 2006; Brown & Wallerstein 1992; Worley et al. 2008, 2010).

Relative to Arcturus, the abundance analyses for these stars give a strong indication for a homogenous distribution of Fe ($\langle$[Fe/H]$\rangle = -0.14 \pm 0.02$ dex), Si ($\langle$[Si/Fe]$\rangle = -0.01 \pm 0.04$ dex) and Ca ($\langle$[Ca/Fe]$\rangle = -0.06 \pm 0.06$ dex) in 47 Tuc. There is a much larger scatter in the abundance derived for Na ($\langle$[Na/Fe]$\rangle = -0.05 \pm 0.14$ dex) and the Na abundance was found to correlate with CN strength. This is a phenomenon also previously observed in 47 Tuc stars (Cottrell & Da Costa 1981; Cannon et al. 2003).

The analysis of the high-resolution spectrum of Lee 2525 determined an enhancement in the Zr abundance for this star [Zr/Fe] = +0.28 dex relative to Arcturus. The medium resolution spectra did not reflect this enhancement ([Zr/Fe] = +0.02 dex relative to Arcturus). The mean Zr abundance (relative to Arcturus) for the survey subset showed an enhancement, $\langle$[Zr/Fe]$\rangle = +0.14 \pm 0.09$ dex, but the large uncertainty is most likely due to the weakness and blending of the measured Zr feature. The mean Ba abundance is $\langle$[Ba/Fe]$\rangle = +0.28 \pm 0.05$ dex, indicative of a homogeneous distribution of this element in 47 Tuc. The spectral features for La and Nd were deemed to be too blended at this resolution for reliable spectrum synthesis analysis, hence this resolution is too low to carry out a comprehensive survey of *s*-process elements in 47 Tuc giant stars.

Most of the light and heavy elements measured in this sample of stars, that all have very similar stellar parameters, have a small spread in values indicating that these elements were most likely created in nuclear processes prior to the formation of these stars. The relation of Na to CN gives the possibility of distinguishing between stellar populations within 47 Tuc. The CN-weak population is typically considered as the initial population, for which the high mass stars have evolved through stellar death and polluted the interstellar medium with products of CNO nulceosynthesis, including the Na enhancement that can be produced through the NeNa cycle. Hence the secondary population are the CN-strong stars. This is consistent with the recent study by Milone et al. (2011), who used precision photometry from HST and ground-based telescopes to identify multiple stellar populations in 47 Tuc. They note 2 major populations with C, N and Na abundance characteristics similar to those found in our study.

The trend of Na and CN can be viewed as a continuum of Na to CN enhancement. From the baseline of enhancement within the initial CN/Na-weak population the CN-strong stars have been further enriched in CN and Na in relative proportions indicating the same process is responsible (CNO cycling via hot bottom burning). However this process was apparently acti-

vated in the CN-strong population, not the CN-weak population. So why do the CN-strong stars have differing degrees of enhancement in CN and Na? Is there another parameter that must be considered? Another consideration is that this sample resides at the connection of the AGB to the RGB. This may provide another distinction with which to understand the spread in CN and Na abundances.

The Lee 2525 sample results of the 47 Tuc giant stars provide an indication about the abundance patterns observed in the light elements. More detailed analysis of the whole sample of 47 Tuc giants will work with the best stellar atmosphere model for each star and to then determine stellar elemental abundances by spectrum synthesis. The heavy elements will require observations at a higher resolution to obtain better detail in the stellar spectra of these typically weak features.

Acknowledgments

CCW and PLC would both wish to acknowledge the hospitality and financial assistance of the Max Planck Institute for Astrophysics which enabled progress to be made on this paper. PLC would also wish to acknowledge the support of the University of Canterbury for his sabbatical during 2011 and a Marsden Fund grant administered by the Royal Society of New Zealand.

This research has made use of the SIMBAD database, operated at CDS, Strasbourg, France and has made use of data products from the Two Micron All Sky Survey, which is a joint project of the University of Massachusetts and the Infrared Processing and Analysis Center/California Institute of Technology, funded by the National Aeronautics and Space Administration and the National Science Foundation.

References

Alonso A., Arribas S., Martínez-Roger C., 1999, A&AS, 140, 261

Briley M. M., Harbeck D., Smith G. H., Grebel E. K., 2004, AJ, 127, 1588

Brown J. A., Wallerstein G., 1992, AJ, 104, 1818

Busso M., Gallino R., Lambert D. L., Travaglio C., Smith V. V., 2001, ApJ, 557, 802

Campbell S. W., Lattanzio J. C., Elliott L. M., 2006, ArXiv Astrophysics e-prints

Campbell S. W., Yong D., Wylie-de Boer E. C., Stancliffe R. J., Lattanzio J. C., Angelou G. C., Grundahl F., Sneden C., 2010, MemSaIt, 81, 1004

Cannon R., da Costa G., Norris J., Stanford L., Croke B., 2003, in Piotto G., Meylan G., Djorgovski S. G., Riello M., eds, New Horizons in Globular Cluster Astronomy Vol. 296 of Astronomical Society of the Pacific Conference Series, Spectroscopy of Main Sequence Stars in Globular Clusters. p. 175

Cannon R. D., Croke B. F. W., Bell R. A., Hesser J. E., Stathakis R. A., 1998, MNRAS, 298, 601

Cottrell P. L., Da Costa G. S., 1981, ApJL, 245, L79

Gratton R., Sneden C., Carretta E., 2004, ARA&A, 42, 385

Hinkle K., Wallace L., 2005, in Barnes III T. G., Bash F. N., eds, Cosmic Abundances as Records of Stellar Evolution and Nucleosynthesis Vol. 336 of Astronomical Society of the Pacific Conference Series, The Spectrum of Arcturus from the Infrared through the Ultraviolet. pp 321–+

Karakas, A. I. and Lugaro, M., 2010, PASA, 27, 227

Lee S. W., 1977, A&AS, 27, 381

Lind K., Asplund M., Barklem P. S., Belyaev A. K., 2011, A&A, 528, A103+

Milone A. P., et al, 2011, ArXiv e-prints, 1109.0900

Norris J., Freeman K. C., 1979, ApJL, 230, L179 (NF79)

Paltoglou G., Freeman K. C., 1984, PhD thesis, Mt. Stromlo and Siding Spring Observatories, Institute of Advanced Studies, Australian National University (PF84)

Reschenhofer E., 2001, Journal of Statistics Education, 9

Sharp R., et al, 2006, in McLean I. S., Masanori I., eds, Ground-based and Airborne Instrumentation for Astronomy Vol. 6269 of Proceedings of the SPIE, Performance of AAOmega: the AAT multi-purpose fiber-fed spectrograph. p. 62690G

Sneden C., 1973, PhD thesis, University of Texas at Austin

Sneden C., Ivans I. I., Kraft R. P., 2000, MemSaIt, 71, 657

Skrutskie, M. F., Cutri, R. M., Stiening, R., Weinberg, M. D., Schneider, S., Carpenter, J. M., Beichman, C., Capps, R., Chester, T., Elias, J., Huchra, J., Liebert, J., Lonsdale, C., Monet, D. G., Price, S., Seitzer, P., Jarrett, T., Kirkpatrick, J. D., Gizis, J. E., Howard, E., Evans, T., Fowler, J., Fullmer, L., Hurt, R., Light, R., Kopan, E. L., Marsh, K. A., McCallon, H. L., Tam, R., Van Dyk, S., Wheelock, S., 2006, ApJ, 131, 1163

Worley C. C., Cottrell P. L., Freeman K. C., Wylie-de Boer E. C., 2009, MNRAS, pp 1471–+

Worley C. C., Cottrell P. L., McDonald I., van Loon J. T., 2010, MNRAS, 402, 2060

Worley C. C., Cottrell P. L., Wylie de Boer E. C., 2008, Publications of the Astronomical Society of Australia, 25, 53

Wylie E. C., Cottrell P. L., Sneden C. A., Lattanzio J. C., 2006, ApJ, 649, 248

A 47 Tuc Giant Star Survey

Table 6: Photometry, effective temperature and surface gravity calculated from V–K, and CN excess calculated in this study for the 97 giant stars in our survey of 47 Tuc.

Star ID	V^*	B–V	V–$K^\#$	$T_{\rm eff}(V$–$K)$	$\log g(V$–$K)$	δC_{2011}
Lee4472	12.40	1.41	0.34	4274	1.44	-0.112
Lee1704	13.00	1.25	-0.89	4827	1.93	-0.045
Pal502	12.64	1.36	3.28	4158	1.27	-0.037
Lee1628	12.94	1.22	2.99	4339	1.50	-0.017
Lee1316/Pal881	13.17	1.17	2.89	4411	1.64	-0.014
Pal1151	13.00	1.25	3.06	4295	1.50	-0.011
Lee2306/Pal388	12.59	1.29	3.07	4288	1.33	-0.005
Lee5601	12.88	1.25	3.06	4292	1.45	-0.001
Lee2428	13.23	1.16	2.96	4360	1.63	0.012
Lee3622/Pal726	12.60	1.31	3.24	4183	1.27	0.014
Lee1506	13.27	1.15	2.87	4423	1.69	0.016
Lee1104/Pal436	13.78	1.08	1.72	4714	2.07	0.017
Lee1312/Pal771	14.48	1.05	2.57	4927	2.46	0.021
Lee1320/Pal925	13.52	1.13	1.57	4509	1.84	0.022
Lee3207/Pal380	13.11	1.22	2.97	4352	1.58	0.028
Lee2608	12.87	1.22	3.07	4285	1.44	0.031
Lee4737	12.96	1.25	3.10	4267	1.46	0.031
Lee4628	12.53	1.31	3.14	4241	1.28	0.043
Lee3305/Pal461	13.03	1.23	3.02	4319	1.53	0.044
Lee1522	13.56	1.08	1.88	4519	1.87	0.046
Lee1423/Pal1124	13.75	1.03	1.68	4761	2.08	0.047
Lee4506	13.54	1.11	1.73	4454	1.82	0.050
Pal1158	13.20	1.13	2.63	4617	1.78	0.052
Lee2616	13.21	1.14	2.84	4448	1.68	0.053
Lee2737	13.51	1.13	1.51	4553	1.87	0.053
Lee2742	13.04	1.08	2.89	4406	1.59	0.059
Lee3404/Pal440	14.53	0.90	2.57	4961	2.49	0.061
Lee2311/Pal500	13.98	0.77	2.02	5708	2.58	0.065
Lee4502	13.28	0.96	-0.51	4468	1.69	0.074
Pal256/Tuc14	14.00	0.85	2.06	5325	2.44	0.075
Lee2310/Pal423	14.50	0.94	2.46	4838	2.42	0.075
Lee1201/Pal507	12.88	1.26	3.10	4266	1.43	0.076
Lee1206/Pal638	14.13	0.84	3.37	5252	2.46	0.076
Lee5705	13.86	1.11	2.42	4505	1.98	0.077
Lee3306/Pal447	14.04	0.90	2.03	5288	2.44	0.079
Lee2525	12.43	1.29	3.16	4232	1.23	0.081
Chu4432/W66	12.55	1.34	3.24	4181	1.25	0.083
Lee1313	14.44	1.00	3.08	4855	2.40	0.084
Lee1105	13.69	1.10	2.46	4598	1.97	0.086
Lee4514	14.35	0.98	2.34	4778	2.33	0.087
Lee1315/Pal869	14.10	0.81	2.85	5297	2.47	0.090
Lee3307	14.23	0.96	2.54	5448	2.58	0.092
Lee3201	13.78	0.88	1.81	5212	2.31	0.093
Lee1529	13.90	0.86	2.80	5118	2.31	0.096
Lee8528	13.72	0.92	2.22	5031	2.20	0.105
Lee8302/Pal1446	14.06	0.85	1.78	5334	2.47	0.106
Pal306/Tuc32	14.02	0.85	2.03	5276	2.43	0.107
Lee1516	13.94	1.04	2.22	4660	2.10	0.110
Lee3312/Pal466	14.11	0.88	1.88	5303	2.48	0.115
Lee1207/Pal5628	14.07	0.84	2.06	5262	2.44	0.127
Lee1735	13.35	1.09	2.76	4505	1.77	0.128
Pal452	12.94	1.24	2.93	4378	1.53	0.131
Lee5703	12.53	1.28	3.17	4221	1.26	0.131
Pal1036	13.95	0.86	2.08	5341	2.43	0.131
Lee2739	13.22	1.18	2.80	4472	1.70	0.132
Lee1513	12.41	1.32	3.14	4242	1.23	0.135
Pal487	13.17	1.15	2.87	4422	1.65	0.139
Lee3205/Pal351	14.07	0.83	2.05	5307	2.46	0.139

Continued on next page

Table 6 – continued from previous page

Star ID	V^*	B–V	V–$K^\#$	$T_{\rm eff}(V$–$K)$	$\log g(V$–$K)$	δC_{2011}
Lee2601	13.83	1.06	3.12	4638	2.04	0.144
Chu4684W139	12.70	1.12	3.17	4223	1.33	0.146
Lee8202/Pal1526	14.08	0.86	3.04	5341	2.48	0.148
Lee3415/Pal368b	14.03	0.86	1.99	5310	2.45	0.149
Lee3403/Pal428	14.03	0.84	2.79	5383	2.48	0.149
Lee2108/Pal342	14.01	0.84	2.47	5347	2.45	0.157
Lee3310/Pal474	14.07	0.85	2.92	5316	2.47	0.158
Lee1301/Pal516	12.64	1.22	2.91	4391	1.42	0.159
Lee2604	13.07	1.04	2.52	4731	1.79	0.161
Lee8508	13.80	0.87	2.19	5006	2.22	0.162
Pal578	13.38	1.14	2.78	4488	1.77	0.164
Pal262/Tuc16	12.72	1.29	3.14	4240	1.35	0.166
Lee4602	13.07	1.19	2.99	4338	1.55	0.167
Lee2201/Pal368a	13.97	0.83	1.90	5351	2.44	0.170
Chu4241/W164	12.62	1.12	3.05	4300	1.35	0.173
Lee3519	14.40	1.02	2.38	4755	2.34	0.174
Lee8301/Pal1353	13.96	0.85	2.33	5334	2.43	0.175
Pal571	13.75	1.08	1.63	4619	2.00	0.175
Lee1319	13.08	0.93	2.28	5037	1.95	0.177
Lee1519	13.89	0.88	3.08	5299	2.39	0.181
Lee1304/Pal506	14.51	0.96	3.38	4794	2.40	0.185
Lee3206/Pal383	14.06	0.84	1.86	5303	2.46	0.186
Lee1309	13.20	1.04	2.61	4635	1.79	0.187
Lee2419/Pal478	14.48	0.96	2.56	4852	2.42	0.194
Lee1324/Pal1125	14.04	0.85	2.13	5287	2.44	0.194
Lee4626	13.27	1.17	2.87	4422	1.69	0.196
Lee4509	12.99	1.21	3.01	4326	1.51	0.198
Lee1408/Pal598	13.49	1.09	2.69	4566	1.87	0.201
Lee2511	13.84	0.84	1.94	5202	2.33	0.201
Pal661	12.54	1.26	3.15	4233	1.28	0.202
Lee1419	14.19	0.97	3.37	4795	2.27	0.208
Lee5717	13.16	1.16	2.94	4372	1.61	0.209
Lee5514	14.15	1.00	2.21	4705	2.21	0.216
Lee1747/S364	12.45	1.26	3.07	4284	1.27	0.223
Lee4636	13.30	1.17	2.78	4493	1.75	0.233
Lee3510	13.63	1.09	2.82	4780	2.04	0.235
Lee4515	14.49	0.98	2.45	4848	2.42	0.262
Lee2302/Pal397	14.07	1.07	2.12	4720	2.19	0.264
Lee2528/Pal625	13.54	1.12	1.52	4532	1.87	0.307

* B&V from SIMBAD
$^\#$ K from 2MASS